Di-Jet Production in Photon-Photon Collisions at $\sqrt{s_{\rm ee}} = 189$ to 209 GeV

T. Wengler[a] for the OPAL collaboration

[a]CERN, EP division, 1211 Geneva 23, Switzerland

Di-jet production is studied in collisions of quasi-real photons at e^+e^- centre-of-mass energies $\sqrt{s_{\rm ee}}$ from 189 to 209 GeV at LEP. The data were collected with the OPAL detector. The structure of jets is investigated and differential cross sections are measured and compared to QCD calculations.

1. Introduction

We have studied the production of di-jets in the collisions of two quasi-real photons at an e^+e^- centre-of-mass energy $\sqrt{s_{\rm ee}}$ from 189 to 209 GeV, with a total integrated luminosity of 593 pb^{-1} collected by the OPAL detector at LEP. Di-jet events are of particular interest, as the two jets can be used to estimate the fraction of the photon momentum participating in the hard interaction, which is a sensitive probe of the structure of the photon. The transverse energy of the jets provides a hard scale that allows such processes to be calculated in perturbative QCD. Fixed order calculations at next-to-leading order (NLO) in the strong coupling constant $\alpha_{\rm s}$ for di-jet production are available and are compared to the data, providing tests of the theory. Leading order Monte Carlo (MC) generators are used to estimate the importance of soft processes not included in the NLO calculation. More details on the results presented here can be found in [1].

The $k_\perp$-clustering algorithm [2] is used as opposed to the cone algorithm [3] in our previous publications [4,5] for the measurement of the differential cross-sections, because of the advantages of this algorithm in comparing to theoretical calculations [6]. The cone jet algorithm is used to demonstrate the different structure of the cone jets compared to jets defined by the $k_\perp$-clustering algorithm.

At e^+e^- colliders the photons are emitted by the beam electrons (positrons). Most of these photons carry only a small negative four-momentum squared, Q^2, and can be considered quasi-real ($Q^2 \approx 0$). The electrons are hence scattered with very small polar angles and are not detected. Events where one or both scattered electrons are detected are not considered in the present analysis.

In LO QCD, neglecting multiple parton interactions, two hard parton jets are produced in $\gamma\gamma$ interactions. In single- or double-resolved interactions, these jets are expected to be accompanied by one or two remnant jets. A pair of variables, x_γ^+ and x_γ^-, can be defined [7] that estimate the fraction of the photon's momentum participating in the hard scattering:

$$x_\gamma^\pm \equiv \frac{\sum_{\rm jets=1,2} (E^{\rm jet} \pm p_z^{\rm jet})}{\sum_{\rm hfs} (E \pm p_z)}, \qquad (1)$$

where p_z is the momentum component along the z axis of the detector and E is the energy of the jets or objects of the hadronic final state (hfs). In LO, for direct events, all energy of the event is contained in two jets, i.e., $x_\gamma^+ = 1$ and $x_\gamma^- = 1$, whereas for single-resolved or double-resolved events one or both values are smaller than 1. Differential cross sections as a function of x_γ or in regions of x_γ are therefore a sensitive probe of the structure of the photon.

2. Jet structure

The internal structure of jets is studied using the jet shape, which is defined as the fractional transverse jet energy contained in a subcone of radius r concentric with the jet axis, averaged

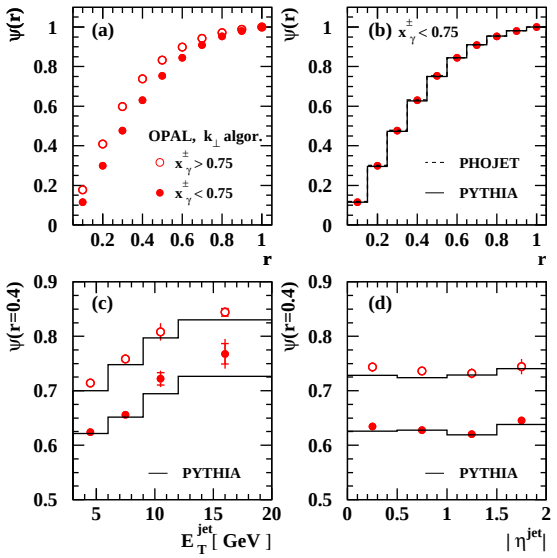

Figure 1. The jet shape, $\Psi(r)$, for the two regions of x_γ^+-x_γ^--space indicated in the figure (a), and $\Psi(r)$ for $x_\gamma^\pm < 0.75$ compared to the predictions of the LO MC generators PHOJET and PYTHIA (b). Figures (c) and (d) show the value of $\Psi(r = 0.4)$ as a function of the transverse energy and pseudo-rapidity of the jet respectively, compared to the PYTHIA prediction.

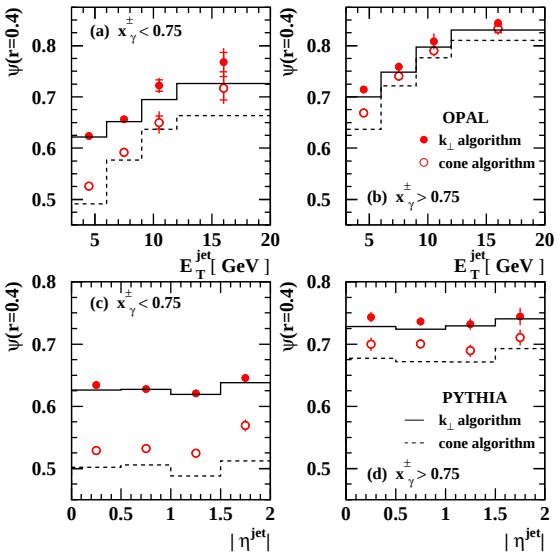

Figure 2. The value of the jet shape $\Psi(r)$ at $r = 0.4$ as a function of the jet transverse energy for $x_\gamma^\pm < 0.75$ (a) and $x_\gamma^\pm > 0.75$ (b), and as a function of the jet pseudo-rapidity for $x_\gamma^\pm < 0.75$ (c) and $x_\gamma^\pm > 0.75$ (d). In each figure the results obtained using the inclusive $k_\perp$ and the cone jet algorithm are shown and compared to the PYTHIA prediction.

over all jets of the event sample:

$$\psi(r) \equiv \frac{1}{N_{\rm jets}} \sum_{\rm jets} \frac{E_{\rm T}^{\rm jet}(r)}{E_{\rm T}^{\rm jet}(r = 1.0)} \qquad (2)$$

with $r = \sqrt{(\Delta\eta)^2 + (\Delta\phi)^2}$ and $N_{\rm jet}$ the total number of jets analysed. Both $k_\perp$ and cone jets are analysed in this way. As proposed in [8], only particles assigned to the jet by the jet finders are considered. Events entering the jet shape distributions are required to have at least two jets with a transverse energy 3 GeV $< E_{\rm T}^{\rm jet} <$ 20 GeV and a pseudo-rapidity $|\eta^{\rm jet}| < 2$.

In Figure 1 (a) the jet shape, $\Psi(r)$, is shown for the $k_\perp$ algorithm for both $x_\gamma^\pm > 0.75$ and $x_\gamma^\pm < 0.75$. Here and in subsequent figures the total of statistical and systematic uncertainties added in quadrature is shown where larger than the marker size. The inner error bars show the statistical errors. The first sample is dominated by direct photon-photon interactions and hence by quark-initiated jets. As is demonstrated in the figure, jets in this sample are more collimated than for small values of $x_\gamma^\pm$, where the cross-section is dominated by resolved processes and hence has a large contribution from gluon-initiated jets. In both cases the jets become more collimated with increasing transverse energy, as is shown in Figure 1 (c). There is no significant dependence on the jet pseudo-rapidity (Figure 1 (d)). Both PHOJET [9] and PYTHIA [10] give an adequate description of the jet shapes as can be seen in Figures 1 (b), (c), and (d). The default choices of SaS 1D [11] for PYTHIA and LO GRV [12] for PHOJET are taken.

Figure 2 compares the shapes of jets defined by the cone algorithm and the $k_\perp$ algorithm, in

each case compared to the shape as obtained from PYTHIA. As for the $k_\perp$-jets, the jets defined by the cone algorithm are more collimated in the quark-dominated sample and always become more collimated for increasing transverse energy, while there is no dependence on the jet pseudo-rapidity. The cone-jets are significantly broader than the jets defined by the $k_\perp$ algorithm at low $E_{\mathrm{T}}^{\mathrm{jet}}$. With increasing $E_{\mathrm{T}}^{\mathrm{jet}}$, jets become more collimated and the two jet algorithms give similar results. While the $k_\perp$-jets are well described by PYTHIA and PHOJET, the jet shapes obtained for the cone-jets are somewhat broader than in the data.

3. Differential Di-jet cross-sections

Only the $k_\perp$ jet algorithm is used for the measurement of the differential di-jet cross-sections. The experimental results are compared to a perturbative QCD calculation at NLO [13] which uses the GRV HO parametrisation of the parton distribution functions of the photon [12], and was repeated for the kinematic conditions of the present analysis. The renormalisation and factorisation scales are set to the maximum $E_{\mathrm{T}}^{\mathrm{jet}}$ in the event. The calculation was performed in the $\overline{\mathrm{MS}}$-scheme with five light flavours and $\Lambda^{(5)}_{\mathrm{QCD}} = 130$ MeV. The average of the hadronisation corrections estimated by PYTHIA and HERWIG have been applied to the calculation for this comparison. In the figures described below the shaded band indicates the theoretical uncertainty estimated by the quadratic sum of two contributions: variation of the renormalisation scale by factors of 0.5 and 2 and the difference between using HERWIG or PYTHIA in estimating the hadronisation corrections.

Due to the different nature of the underlying partonic process one expects different distributions of the angle Θ^* between the jet axis and the axis of the incoming partons or direct photons in the di-jet centre-of-mass frame. The leading order direct process $\gamma\gamma \to \mathrm{q\bar{q}}$ proceeds via the t-channel exchange of a spin-$\frac{1}{2}$ quark, which leads to an angular dependence $\propto \left(1-\cos^2\Theta^*\right)^{-1}$. In double resolved processes the sum of all matrix elements, including a large contribution from spin-1 gluon exchange, leads to an approximate angular dependence $\propto (1-|\cos\Theta^*|)^{-2}$ [14]. The contribution of the different processes to all resolved events depends on the parton distribution functions of the photon. An estimator of the angle Θ^* can be formed from the pseudo-rapidities of the two jets as

$$\cos\Theta^* \;=\; \tanh\left(\frac{\eta_1^{\mathrm{jet}} - \eta_2^{\mathrm{jet}}}{2}\right), \qquad (3)$$

where it is assumed that the jets are collinear in ϕ and have equal transverse energy. Only $|\cos\Theta^*|$ can be measured, as the ordering of the jets in the detector is arbitrary. To obtain an unbiased distribution of $|\cos\Theta^*|$ the measurement needs to be restricted to the region where the di-jet invariant mass $M_{\mathrm{jj}} = 2\bar{E}_{\mathrm{T}}^{\mathrm{jet}}/\sqrt{1-|\cos\Theta^*|^2}$ is not influenced by the cuts on $E_{\mathrm{T}}^{\mathrm{jet}}$ [5]. In the present analysis a cut of $M_{\mathrm{jj}} > 15$ GeV ensures that the $|\cos\Theta^*|$ distribution is not biased by the restrictions on $E_{\mathrm{T}}^{\mathrm{jet}}$ for the range $|\cos\Theta^*|<0.8$ and $|\bar{\eta}^{\mathrm{jet}}| = |\left(\eta_1^{\mathrm{jet}} + \eta_2^{\mathrm{jet}}\right)/2| < 1$ confines the measurement to the region where the detector resolution on $|\cos\Theta^*|$ is good.

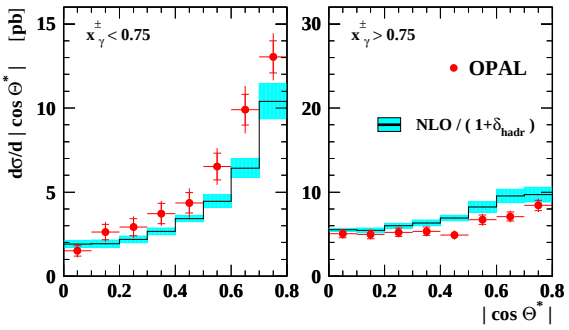

Figure 3. The di-jet cross-section as a function of $|\cos\Theta^*|$ for the two regions in x_γ^+-x_γ^--space indicated in the figure.

Figure 3 shows the differential di-jet cross-section as a function of $|\cos\Theta^*|$ for both $x_\gamma^\pm > 0.75$ and $x_\gamma^\pm < 0.75$. The steeper rise with increasing $|\cos\Theta^*|$ from the dominating spin-1 gluon exchange in the second sample is clearly vis-

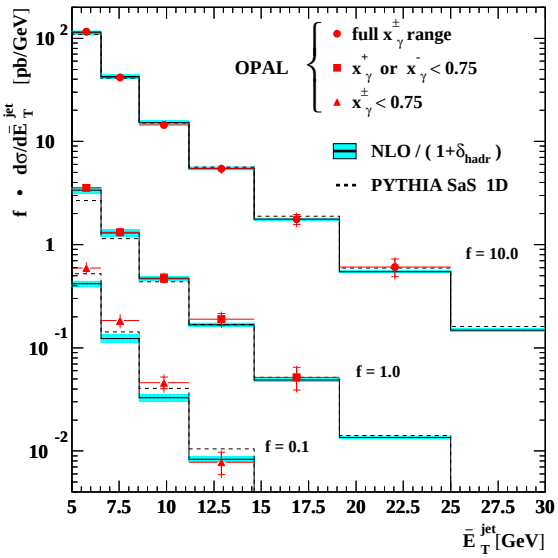

Figure 4. The di-jet cross-section as a function of the mean transverse energy $\bar{E}_{\mathrm{T}}^{\mathrm{jet}}$ of the di-jet system, for the three regions in x_γ^+-x_γ^--space given in the figure. The factor f is used to separate the three measurements in the figure more clearly.

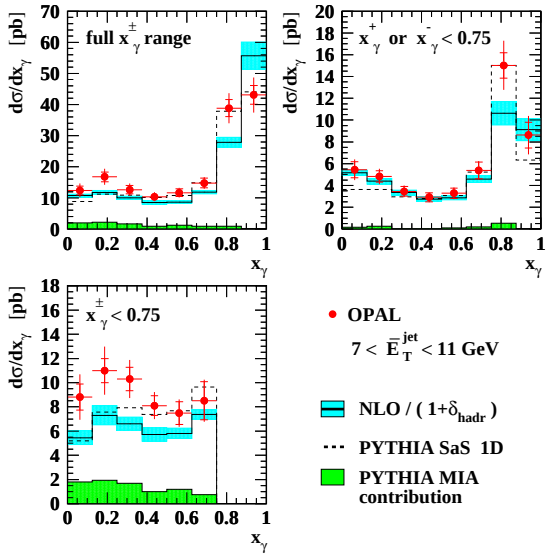

Figure 5. The di-jet cross-section as a function of x_γ and for the regions of the mean transverse energy $\bar{E}_{\mathrm{T}}^{\mathrm{jet}}$ and $x_\gamma^\pm$ of the di-jet system indicated in the figures.

ible. The shape of both samples is well described by NLO QCD. For $x_\gamma^\pm < 0.75$ the NLO calculation is about 20 % below the data. It should be noted that in this region the contribution from the underlying event, not included in the calculation, is expected to be largest, as discussed in more detail below. For $x_\gamma^\pm > 0.75$ the NLO QCD prediction is about 20 % above the data. While here the contribution from MIA is small, this region is affected by rather large hadronisation corrections, which translates into an uncertainty of the normalisation in comparing the theoretical prediction to the data. Probably more importantly it has been pointed out that the calculation of the cross section becomes increasingly problematic when approaching $x_\gamma = 1$ [15].

The differential di-jet cross-section as a function of the mean transverse energy $\bar{E}_{\mathrm{T}}^{\mathrm{jet}}$ of the di-jet system is shown in Figure 4. At high $\bar{E}_{\mathrm{T}}^{\mathrm{jet}}$ the cross-section is expected to be dominated by direct processes, associated with the region $x_\gamma^\pm > 0.75$. Consequently we observe a significantly softer spectrum for the case $x_\gamma^\pm < 0.75$ than for the full x_γ^+-x_γ^--space. The calculation is in good agreement with the data for the full x_γ^+-x_γ^--range and for x_γ^+ or $x_\gamma^- < 0.75$. The cross-section predicted for $x_\gamma^\pm < 0.75$ is again below the measurement. PYTHIA 6.161 is in good agreement with the measured distributions using the SaS 1D parton densities.

The three plots of Figure 5 show the differential cross section as a function of x_γ for the three regions in x_γ^+-x_γ^--space described above. The shaded histogram on the bottom of each of the three plots indicates the contribution of MIA to the cross section as obtained from the PYTHIA [10] MC generator. It is evident especially for $x_\gamma^\pm$<1 that the MIA contribution is of about the same size as the discrepancy between the measurement and the NLO prediction. Furthermore it is interesting to observe that there is next to no MIA contribution to the cross section if either x_γ^+ or x_γ^- is required to be less than one,

while the sensitivity to the photon structure at small x_γ is retained. As one would expect also the agreement of the NLO calculation with the measurement is best in this case. With these measurements one is therefore able to disentangle the hard subprocess from soft contributions and make the firm statement that NLO perturbative QCD is adequate to describe di-jet production in photon-photon collisions in the regions of phase space where the calculation can be expected to be complete and reliable, i.e. where MIA contributions are small and for x_γ not too close to unity. At the same time a different sub-set of observables can be used to study in more detail the nature of the soft processes leading to the underlying event.

REFERENCES

1. OPAL Collaboration, G. Abbiendi et al. *Di-Jet Production in Photon-Photon collisions at sqrt(s)ee from 189 to 209 GeV*, CERN-EP-2002-093, Submitted to Eur. Phys. J.
2. S. Catani, Yu.L. Dokshitzer, M.H. Seymour and B.R. Webber, Nucl. Phys. B406 (1993) 187; S.D. Ellis, D.E. Soper, Phys. Rev. D48 (1993) 3160.
3. OPAL Collaboration, R. Akers et al., Z. Phys. C63 (1994) 197.
4. OPAL Collaboration, K. Ackerstaff et al., Z. Phys. C73 (1997) 433.
5. OPAL Collaboration, G. Abbiendi et al., Eur. Phys. J. C10 (1999) 547.
6. M. Wobisch and T. Wengler, hep-ph/9907280; M.H. Seymour, hep-ph/9707349; S.D. Ellis, Z. Kunszt and D.E. Soper, Phys. Rev. Lett. 69 (1992) 3615.
7. L. Lönnblad and M. Seymour (convenors), $\gamma\gamma$ *Event Generators*, in "Physics at LEP2", CERN 96-01, eds. G. Altarelli, T. Sjöstrand and F. Zwirner, Vol. 2 (1996) 187.
8. M.H. Seymour, Nucl. Phys. B513 (1998) 269.
9. R. Engel, Z. Phys. C66 (1995) 203; R. Engel and J. Ranft, Phys. Rev. D54 (1996) 4244.
10. T. Sjöstrand, Comp. Phys. Comm. 82 (1994) 74; T. Sjöstrand, LUND University Report, LU-TP-95-20 (1995).
11. G.A. Schuler and T. Sjöstrand, Z. Phys. C68 (1995) 607.
12. M. Glück, E. Reya and A. Vogt, Phys. Rev. D45 (1992) 3986; M. Glück, E. Reya and A. Vogt, Phys. Rev. D46 (1992) 1973.
13. M. Klasen, T. Kleinwort and G. Kramer, Eur. Phys. J. Direct C1 (1998) 1; B. Pötter, Eur. Phys. J. Direct C5 (1999) 1.
14. for example: H. Kolanoski, *Two-Photon Physics at e^+e^- Storage Rings*, Springer-Verlag (1984); B.L. Combridge, J. Kripfganz and J. Ranft, Phys. Lett. B70 (1977) 234; D.W. Duke and J.F. Owens, Phys. Rev. D26 (1982) 1600.
15. L. Bertora and S. Frixione, these proccedings.